MNRAS **000**, 1–?? (year) Preprint 18 May 2016 Compiled using MNRAS LATEX style file v3.0

Core and Conal Component Analysis of Pulsar B1933+16 — Investigation of the Segregated Modes

Dipanjan Mitra[1,2,3] Joanna Rankin[1,4] & Mihir Arjunwadkar[5]
[1] *Physics Department, University of Vermont, Burlington, VT 05405*⋆
[2] *National Centre for Radio Astrophysics, Ganeshkhind, Pune 411 007 India*†
[3] *Janusz Gil Institute of Astronomy, University of Zielona Góra, Lubuska 2, 65-265 Zielona Góra, Poland*
[4] *Sterrenkundig Instituut 'Anton Pannekoek', University of Amsterdam, NL-1090 GE*
[5] *Centre for Modeling and Simulation, Savitribai Phule Pune University, Ganeshkhind, Pune 411 007 India*‡

arXiv:1605.05010v1 [astro-ph.HE] 17 May 2016

In original form year month day

ABSTRACT

Radio pulsar B1933+16 is brightest core-radiation dominated pulsar in the Arecibo sky, and here we carry out a comprehensive high resolution polarimetric study of its radiation at both 1.5 and 4.6 GHz. At 1.5 GHz, the polarization is largely compatible with a rotating-vector model with α and β values of 125 and –1.2°, such that the core and conal regions can be identified with the primary and secondary polarization modes and plausibly with the extraordinary and ordinary propagation modes. Polarization modal segregation of profiles shows that the core is comprised of two parts which we associate with later X-mode and earlier O-mode emission. Analysis of the broad microstructures under the core shows that they have similar timescales to those of the largely conal radiation of other pulsars studied earlier. Aberration/retardation analysis was here possible for both the conal and core radiation and showed average physical emission heights of about 200 km for each. Comparison with other core-cone pulsars suggests that the core and conal emission arises from similar heights. Assuming the inner vacuum gap model, we note that at these emission altitudes the frequency of the observed radiation ν_{obs} is less than the plasma frequency ν_p. We then conclude that the radio emission properties are consistent with the theory of coherent curvature radiation by charged solitons where the condition $\nu_{obs} < \nu_p$ is satisfied. However, the differences that exist between core and conal emission in their geometric locations within a pulse, polarization and modulation properties are yet to be understood.

Key words: – pulsars: B1933+16, polarization, non-thermal radiation mechanisms

1 INTRODUCTION

Radio pulsar B1933+16 is the brightest core-emission dominated pulsar in the Arecibo sky, as the majority of such pulsars fall far in the southern sky around the Galactic center. Despite its prominence, it has received very little study and analysis. Sieber *et al.* (1975) early showed its profile evolution from a single form at meter wavelengths to a tripartite one above 1 GHz, and this pattern of evolution later became a defining characteristic of the core-single profile class in the *Empirical Theory of Pulsar Emission* series (Rankin 1983, 1993a; hereafter ET I, VIa). Other work (Gould & Lyne 1998; Rankin, Stinebring & Weisberg 1989; Weisberg *et al.* 1999; Hankins & Rankin 2010) confirmed this profile evolution with even better quality observations.

In the parlance of the ET papers, B1933+16 has been regarded as having a core-single ($\mathbf{S}_t$) profile, meaning that it "grows" conal "outriders" only at high frequency. The star's core feature does exhibit the antisymmetric circular polarization often seen under core features, as we see in Fig. 1 below, and the angular dimensions of the core and conal components seem to reflect the angular size of the pulsar's polar cap emission region as expected in ET VI. However, B1933+16's core "component" does exhibit a very clear non-Gaussian structure—as do some other core features (sometimes earlier referred to as "notches")—and its origin is one of the questions before us below. At lower frequencies its core component gradually broadens (ET II), in part because of scattering, and by 100 MHz, the scattering tail occupies the entire rotation cycle (Izvekova *et al.* 1989).

Few pulse-sequence analyses had been carried out on pulsars with dominant core emission. Exceptions are B0329+54 and the Vela pulsar B0833–45, the study of this

⋆ dmitra@uvm.edu; Joanna.Rankin@uvm.edu
† dmitra@ncra.tifr.res.in
‡ mihir@cms.unipune.ac.in

© year The Authors

latter pulsar by Krishmohan & Downs (1983) being an early classic which has received far too little followup. Our study of B0329+54's normal mode (Mitra, Rankin & Gupta 2007) revealed a clear signature of intensity-dependent aberration/retardation (hereafter A/R) in its core emission, which in turn was interpreted as the presence of a linear amplifier within the star's polar flux tube. A further study showing similar core properties was conducted with pulsar B1237+25 (Smith, Rankin & Mitra 2012).

Johnston *et al.* (2005) first demonstrated that the "fiducial" polarization orientation of pulsar radio emission—at the central longitude of the magnetic axis—exhibits preferential parallel or orthogonal alignments with respect to their proper-motion (hereafter PA_v) directions. In carrying this work further by considering only pulsars with core emission, Rankin (2015) showed that the later core emission shows an accurate orthogonal orientation reflecting the extraordinary X propagation mode. The classic Johnston *et al.* study did include pulsar B1933+16; but, in their analysis its alignment was indifferent. We have come to believe, however, that the longitude of the pulsar's magnetic axis falls later than was then thought, and when this is taken into account, B1933+16's late core emission seems to be the X mode and, if so, the two polarization modes can be identified throughout its profile. This will be further discussed below.

In this current analysis we have a few straightforward objectives that follow from our earlier pulse-sequence analyses of core emission above: a) we want to assess whether the star's core radiation exhibits intensity-dependent A/R and, if so, interpret its physical significance; b) we will attempt to understand how the pulsar's polarization position-angle (hereafter PPA) traverse becomes distorted from what would be expected from the rotating-vector model (hereafter RVM; Radhakrishnan & Cooke 1969); we want to understand the significance of the pulsar's prominent circular polarization; further, B1933+16 is one of the few bright pulsars available to us in which core microstructure can be investigated, so we will attempt an analysis similar to that of Mitra, Arjunwadkar & Rankin (2015); and finally we will assess how the pulsar's conal emission is connected to its prominent core radiation.

In what follows, §2 describes our observations. §3 presents our polarimetry, and §4 discusses the results of intensity fractionation. In §5 we conduct analyses of the segregated modes, §6 interprets the PPA traverse geometrically, and §7 presents the microstructure analysis. §8 discusses the core and conal emission, §9 provides an aberration/retardation analysis, and §10 considers the frequency independence of the modal polarization. §12 then summarizes our results and §13 considers their larger theoretical interpretation and significance.

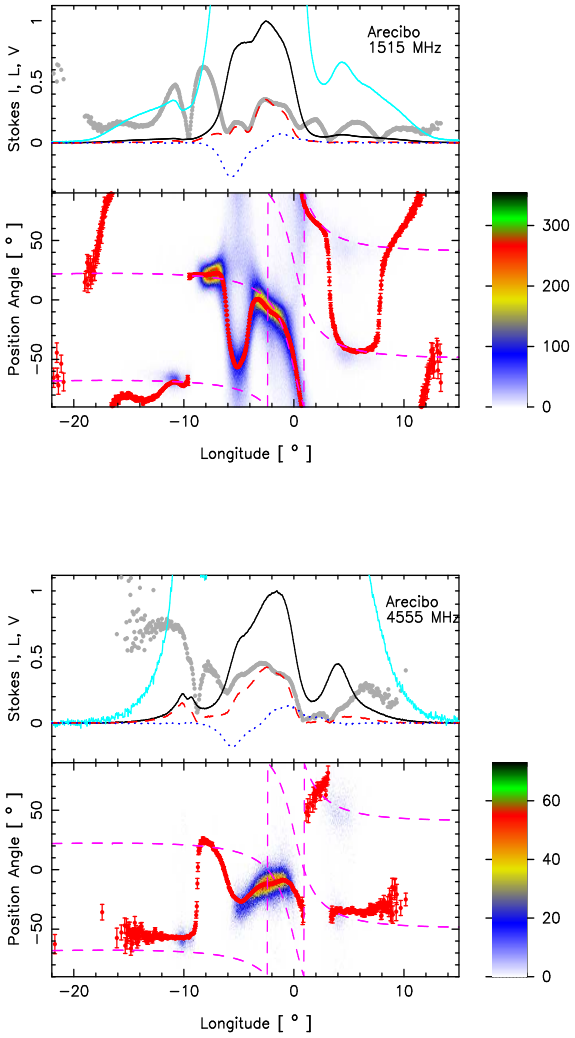

Figure 1. Total polarization displays at 1515 MHz (top) and 4555 MHz (bottom), giving (upper panels) the total intensity (Stokes I; solid curve), the total linear (L ($=\sqrt{Q^2+U^2}$); dashed red), the circular polarization (Stokes V; dotted blue), the fractional linear polarization (L/I; gray points) and a zoomed total intensity ($10\times I$; cyan curve). The PPA [$=\frac{1}{2}\tan^{-1}(U/Q)$] densities (lower panels) within each 1°x1-sample cell correspond to samples larger than 2 σ in L, are plotted according to the color bars at the lower right, and have been derotated to infinite frequency. The average PPA traverses (red) are overplotted, and the RVM fit to the 1515-MHz PPA traverse is plotted twice for the two polarization modes (magenta dashed) on each panel. The origin is taken at the fitted PPA inflection point.

2 OBSERVATIONS

The observations used in our analyses were made using the 305-m Arecibo Telescope in Puerto Rico. The primary 1515-MHz polarized pulse sequence (hereafter PS) was acquired with the upgraded instrument using seven Mock Spectrometers on 2015 April 7 (MJD 57119) and is comprised of 5017 pulses. Each spectrometer sampled a 25-MHz portion of the 275-MHz band centered at 1515 MHz with 36.14 μs sampling. The 4555-MHz observation was again carried out using seven Mocks on 2015 September 20 (MJD 57284) with a total bandwidth of 7x150 MHz and 51 μs sampling. The Stokes parameters have been corrected for dispersion, interstellar Faraday rotation and various instrumental polarization effects and are ultimately derotated to infinite frequency. Errors in the PPAs were

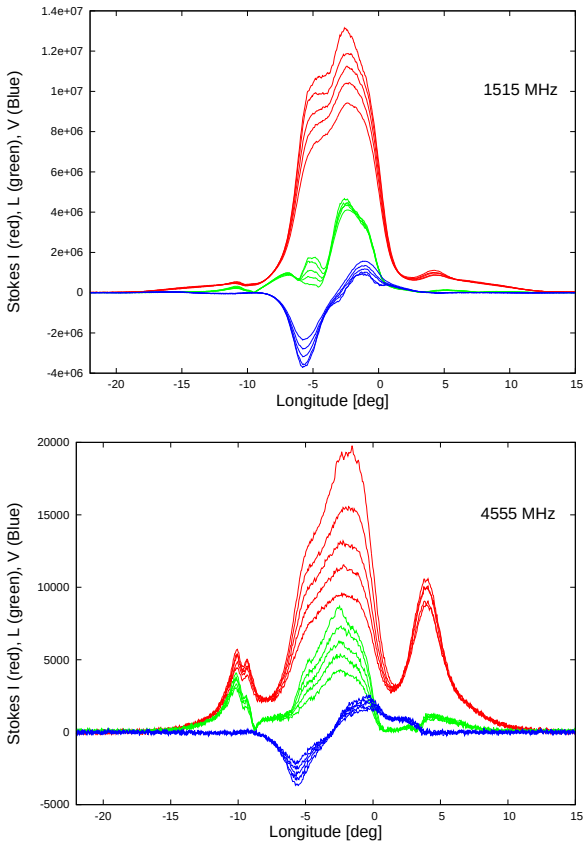

Figure 2. Average profiles corresponding to five intensity fractions for the 1.5-GHz (upper) and 4.6-GHz (lower) observations. Overall, this analysis reflects the steadiness of the pulsar's emission. However, several aspects are worthy of mention. Note the manner in which the leading part of the core becomes progressively weaker relative to the trailing region with increased intensity. Also, note that this leading part becomes more linearly polarized.

computed relative to the off-pulse noise phasor—that is, $\sigma_{PPA} \sim tan^{-1}(\sigma_{off-pulse}/L)$.

3 CONFRONTING THE POLARIMETRY

The average 1515- and 4555-MHz polarimetry presented in Fig. 1 is new and unique in several ways. First, the pulsar is strong enough that a large proportion of the respective 36 and 51-μs samples show well defined polarization—and the linear polarization angle (hereafter PPA) histograms corresponding to them are plotted in the lower panels along with the average PPA traverse. The histograms also have the effect of revealing the polarized structure of the 1.5-GHz PPA "notch" at –5° much more clearly, as in earlier profiles it is seen only a "bump" in the average PPA traverse. The PPAs have been derotated to infinite frequency, so that it is easy to see that several "patches" of PPAs at the two frequencies correspond to each other.

The puzzling structure of the central core component is clear in the total power profiles at both frequencies (solid black curves), and while earlier noted as a "notch" possibly due to "absorption", we will explore whether it has a different origin. The aggregate linear polarization (dashed red) is only moderate at both frequencies across the full width of the profile, and we see a consistent signature of circular polarization (dotted blue). The conal outriding components are more prominent at the higher frequency as expected, and PPA "patches" corresponding to their orthogonal polarization modes (hereafter OPMs) fall at similar positions in the respective lower panels.

Only at the lower frequency is it possible to fit a rotating-vector model (hereafter RVM) traverse to the observed PPAs. The fit is simultaneous to both modes, and the fitted PPA trajectory is shown by a pair of magenta curves. The primary mode track is seen at a PPA of +20° near the leading edge of the plot and rotates negatively through about 160° to +41° on the far right of the plot. The longitude origin of the plot is then taken at the inflection point, and the PPA here is about –58°. This fitted track seems very plausible in terms of the array of 1.5-GHz PPA "patches", but it is important to resolve whether it is both unique and correct. Of course, we have had to omit the non-RVM PPAs around –5° longitude from the fitting, and we clearly see pairs of other "patches" on the conal edges of the profile. We explored, for instance, whether the core PPAs from about –9 to 0° might represent the same mode as the main conal "patch" at 5-6°, and we found not surprisingly that the total PPA traverse is not large enough to fit these under any conditions. So, our conclusion is that most of the core power represents one mode, whereas the –5° region and the brighter emission under the conal outriders the other.

The RVM fit to the 1.5-GHz PPA cannot constrain α and β values due to the large correlation of about 98% between them (see for e.g. Everett & Weisberg 2001). However, the fitted slope R_{PA} [$=\sin\alpha/\sin\beta$] of –39±3 °/° and PPA at the inflection point of –58°±5° are well determined, and the longitude origin is taken at this point in the plots. The other way of estimating α comes from the core-width measurement as was done in ET VI. Using this α (see section 6 and 11) as initial value to the fits we obtained α and β values of 125°±19° and –1.2°±0.5°, where the errors correspond to the fit errors. We were unable to carry out a similar fitting for the 4.6-GHz observation—as is pretty obvious from the nature of the polarized profile. However, we were able to "anchor" the lower frequency solution on its prominent leading and trailing PPA "patches" and the PPA curve is plotted as in the lower frequency profile.

That the fitted PPA inflection point falls so late under the core feature initially surprised us, but we then recalled that we have seen this behavior under core features in faster pulsars. With a rotation period of 359 ms, we suspect that this is due to aberration/retardation (hereafter A/R) which we will explore further below.

Similarly, we were perplexed by the orientation of the inflection-point PPA (PA_0) as one of us had recently interpreted it as –87° (Rankin 2015) on the basis of the Johnston *et al.*'s (2005) average polarimetry. Surely this gives an object lesson regarding the difficulties of interpreting average PPA traverses without appeal to any pulse-sequence polarimetry. Here we find a PA_0= –58°±5°, and we can use this value to estimate the orientation of the pulsar's rotation axis on the sky so as to then determine how the radiation is polarized with respect to the emitting magnetic field direc-

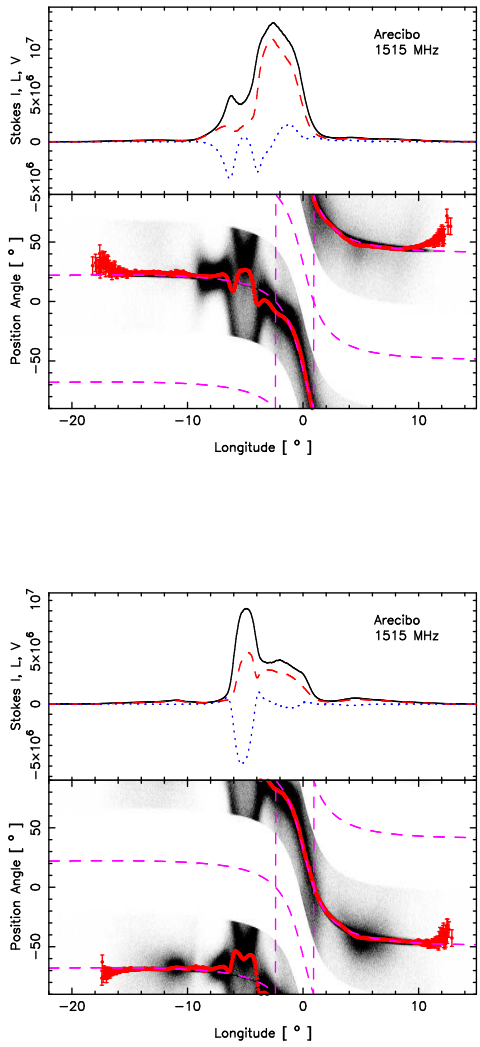

Figure 3. Polarization profiles and PPA distributions after Figure 1 for two-way polarization-mode PS segregations of the 1.5-GHz observation per Deshpande & Rankin (2001); primary mode (top) and secondary mode (bottom).

tion. Pulsar proper motions have been found to be largely parallel to a pulsar's rotation axis (Rankin 2015), and that of B1933+16 was determined by VLBI to be $PA_v = +176(0)^\circ$. A similar value was given by Johnston *et al.* as an improved estimate over that determined earlier by Hobbs *et al.* (2004). Therefore, the alignment angle $\Psi = PA_v - PA_0$ is computed $-4 - (-58) = +54^\circ \pm 5^\circ$, modulo 180°. Although this value is far from orthogonal, we will interpret it as corresponding to the extraordinary (X) propagation mode.

Indeed, the compact distribution of Ψ values (*e.g.,* Rankin 2015) is surprising as there are a number of effects that would tend to misalign a pulsar's rotation and proper motion direction even if the natal "kicks" are initially aligned (*e.g.,* Johnston *et al.* 2005). Noutsos *et al.* (2012) in particular note the effects of binary disruption which might impose a large velocity component orthogonal to the rotation direction. We know little about B1933+16's specific origins or natal binary system, but it is worth noting that there are four known pulsars within a degree or so of it and at about the same dispersion measure. So, the canted Ψ value above should not immediately be taken as evidence against our association of its primary core emission with the X mode. We clearly have much yet to learn both about why Ψ values tend to close alignment and why they depart from said.

4 INTENSITY FRACTIONATION OF THE TOTAL POLARIZED PROFILES

Fig. 2 gives intensity-fractionated average profiles for the two observations. The 1.5-GHz display in the upper plot exhibits rather little change, showing that the pulsar's emission is very steady from pulse to pulse. There is not enough intensity variation in its pulses to show large differences. This said, we can see a subtle but consistent pattern at both frequencies: the leading portion of the core feature becomes slightly but progressively weaker relative to the trailing portion with increased intensity. Note also that while the aggregate linear power in the trailing portion of the 1.5-GHz profile depends little on intensity, the leading portion shows an increase.

5 SEGREGATING THE POLARIZATION MODES

In order to better study the physical emission properties, we next segregate the modal emission in the 1.5-GHz PS into two sequences. The procedures for the operations were discussed in Deshpande & Rankin (2001; Appendix), and here we first consider the two-way segregation, which implicitly assumes that the depolarization is modal in origin, and thus the procedure partially repolarizes the modal sequences. Average profiles corresponding to the two modes are given in Fig. 3, where the primary polarization mode (PPM) is plotted in the upper panels and the secondary (SPM) in the lower ones. Dashed (magenta) RVM curves corresponding to the OPMs are indicated, and the respective regions of polarized samples contributing to the average profiles (exceeding a 2-σ threshold) clearly shown.

This polarization-modal segregation shows that the trailing portion of the core feature plays the strongest role in the PPM and the leading in the SPM. We also see that most of the conal power is in the SPM. The two-way modal partial profiles in Fig. 3 are repolarized following the assumption that the total profile is depolarized due only to the effects of the two orthogonal polarization modes ; however, the three-way modal segregations in Fig. 4 are polarized similarly on their own, suggesting that the assumption is not wrong.

This all said, it is the large negative 'U'-shaped traverse of the PPA in the 1.5-GHz profile at –5° that draws the eye. This feature is much more prominent in this observation than any other previous one because of its high resolution—and thus minimal mode mixing within individual samples. Many other average profiles show only a "bump" at this point (*e.g.,* see Johnston *et al.* 2005). We here see that the

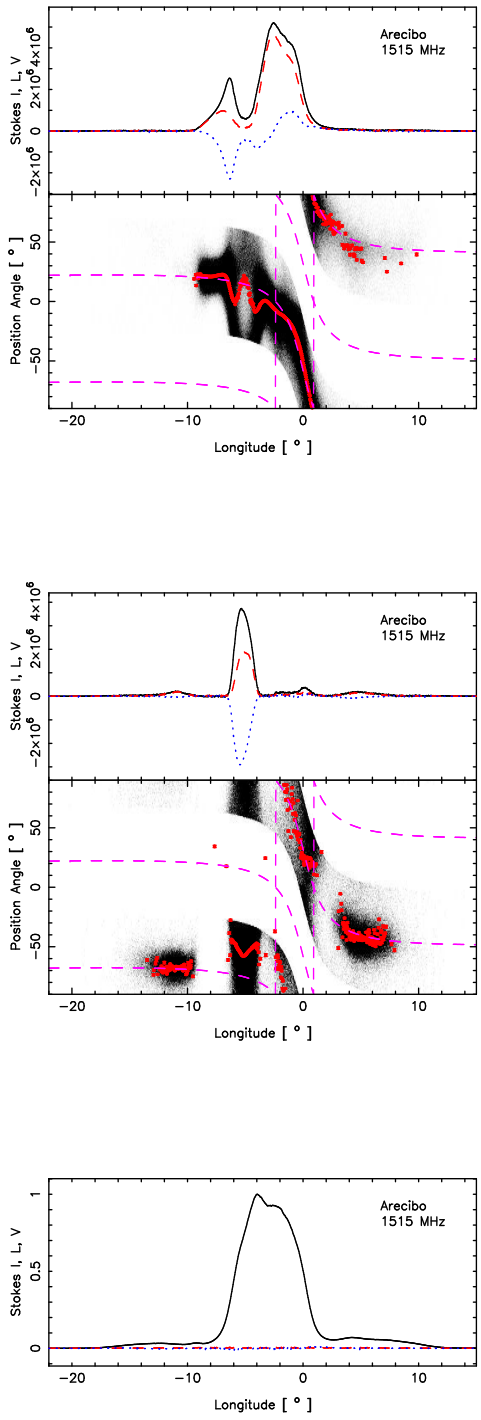

Figure 4. Polarization profiles and PPA distributions after Figure 1 for three-way polarization-mode PS segregations of the 1.5-GHz observation per Deshpande & Rankin (2001); primary mode (top), secondary mode (middle) and unpolarized (bottom). PPA samples larger than 5σ in the linear polarization are plotted in the histogram.

source of this abrupt shift in the average PPA is an aberrant "patch" of PPAs at about –50°, which falls close to, but apparently just above, the SPM modal track. Moreover, the adjacent regions are unusually prominent here just because of the non-orthogonality of the –50° power, as linear polarization mixing within even these highly resolved samples tends to result in systematically progressive PPAs.

This interesting configuration is prominent in all of our analyses in different ways: in the 1.5-GHz total average profile of Fig. 1, one can see that the depolarization around –5° longitude results from PPAs of almost every value. At 4.6-GHz the situation is less clear because there are so many fewer qualifying PPA values. In the two-way segregations of Fig. 3, the repolarization code produces an artifact primarily in the SPM. Only in the upper two panels of the three-way segregations do we see a fairly clear indication of the actual PPA populations here.

The three-way segregations thus give the clearest picture of the polarization-modal structure of the profile in the –5° region: the SPM power in the middle display fits precisely into the region where PPM power is missing in the top display. Weak positive circular polarization is associated with the trailing part of the core; however, the leading SPM power in the middle display is almost completely negatively circularly polarized.

6 INTERPRETING THE EMISSION GEOMETRY

Although the 1.5-GHz polarization display in Fig. 1 shows a PPA distribution of unusual complexity (and one is initially at pains to understand what the 4.6-GHz PPA "patches" have to do with the RVM fit at all!), we believe the RVM fitting to the PPAs in the 1.5-GHz observation is correct and consistent in the following ways: First, exempting the region around longitude –5°, we can follow a PPA trajectory under the core feature that begins near –9°, sweeps strongly negative under the trailing edge of the core and includes the weaker trailing conal PPA "patch" at some +45°. We already noted that an RVM curve cannot be fitted if the brighter trailing patch is included. The RVM fit then gives an inflection near –58°. Second, note that the bright conal PPA "patches" both fall near the SPM curve. And third, we see that the PPM inflection point falls near the midpoint or average of the two SPM conal "patches" as it must if the RVM model is to be consistent for both the core and conal regions.

At 4.6 GHz, we have much less to go on. If this were the only profile available, no sound interpretation could be made. However, we note that the three conal PPA "patches", one leading and the two trailing, fall at nearly identical positions in the PPA distributions of Fig. 1 that have been derotated to infinite frequency. So it is the core region that is mainly different, but even here the PPA "patch" at about –1° falls at about the same place at the two frequencies.

The effort in ET VI to interpret B1933+16's geometry confronted the non-Gaussian shape of the pulsar's central feature and remarkably took twice the peak-to-trailing edge distance, some 4.3°, as the "core width" corresponding to the observed angular diameter of the polar cap. α, β estimates of 72° and 1.1° followed which are trivially different

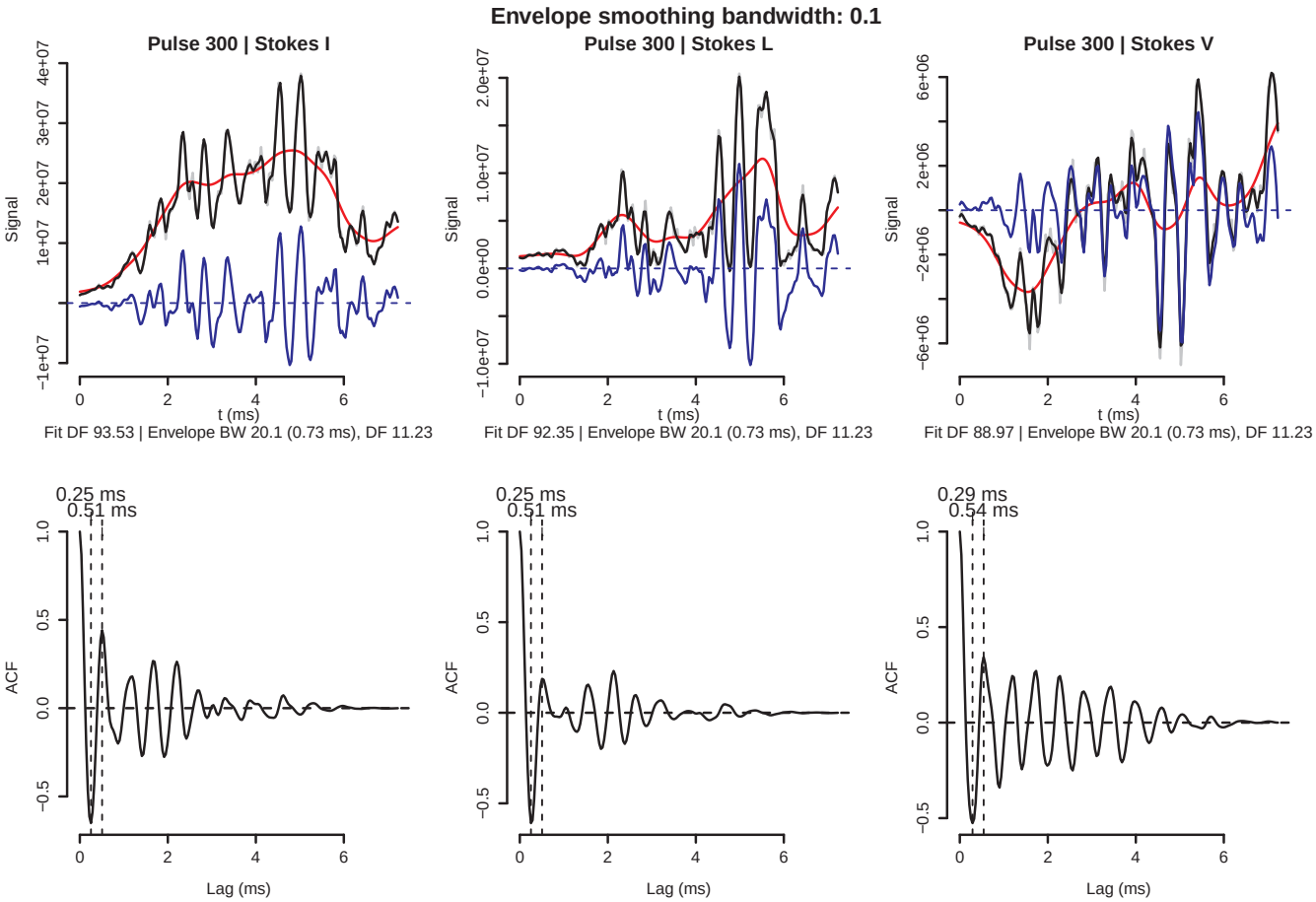
Envelope smoothing bandwidth: 0.1
Pulse 300 | Stokes I
Pulse 300 | Stokes L
Pulse 300 | Stokes V
Signal
t (ms)
Fit DF 93.53 | Envelope BW 20.1 (0.73 ms), DF 11.23
Fit DF 92.35 | Envelope BW 20.1 (0.73 ms), DF 11.23
Fit DF 88.97 | Envelope BW 20.1 (0.73 ms), DF 11.23
0.25 ms
0.51 ms
0.25 ms
0.51 ms
0.29 ms
0.54 ms
ACF
Lag (ms)

Figure 5. Three examples of our analysis methods for extracting subpulse timescales in the 1.5-GHz core emission, and the three columns correspond to Stokes I, L and V. This is similar to MAR15's fig. 5, but here only the smoothing bandwidth $h = 0.1$ is shown. The grey lines in the uppermost panels show the subpulse amplitudes, the fits to them (black lines), the envelopes (red lines), and the microstructure signal (blue lines), computed as the difference between the subpulse amplitude and envelope. The second panel shows the ACF of the microstructure signal. For a detailed description of the technique refer to MAR15.

that the 125° (using the Everett & Weisberg convention) determined by the RVM fitting above. The paper's discussion passed over in silence how the unresolved leading feature might be interpreted.

The dramatic increasing prominence of B1933+16's conal outrider pair leaves little doubt, then, that its high frequency profiles represent a core/cone configuration, but it is less clear just how to classify it. As we have seen in the 1.5-GHz profile, the conal power is very broadly distributed and does not consist in neat components. Paper ET VI then gave B1933+16 as a rare example of a core triple $\mathbf{S}_t$ pulsar with outer conal outriders, but its closer, better defined conal components at 4.6 GHz defeat this interpretation. Notice the very different shapes and extents of the conal components at the two bands in Fig. 1. Although no clear double-cone structure can be discerned, the conal emission is so broad at 1.5-GHz (extending over some 30° with half-power points around 22°), that outer conal power must dominate at this frequency. Further, broad conal power can be seen in the recent 775-MHz profile of Han *et al.* (2009), such that the pulsar could be regarded as having a triple **T** or even five-component **M** profile. However, these sometimes "fuzzy" 1-GHz profile classes all reflect and illuminate the underlying core/double-cone structure of pulsar radio emission beams.

In any case, using the best determined values of α, β and R_{PA} above, the observed angular diameter of the polar cap would be 5.0°, and the roughly 16° outside half-power width of the conal outriders at 4.6 GHz definitely identifies them as having the dimensions of an inner conal beam. Thus using this profile-width information together with R_{PA} and the quantitative geometry of Paper ET VI permits us to confirm that the fitted alpha and beta values were close to correct.

7 MICROSTRUCTURE PROPERTIES

The bright single pulses of PSR B1933+16 in conjunction with the high time resolution made possible by the Arecibo observations provide an ideal context for studying the properties of microstructures in this pulsar. Close visual inspection of single pulses at both 1.5 and 4.5 GHz reveals that the bright core component is rich in small timescale fluctuations in all the Stokes parameters akin to the broad microstructures recently studied by Mitra, Arjunwadkar &

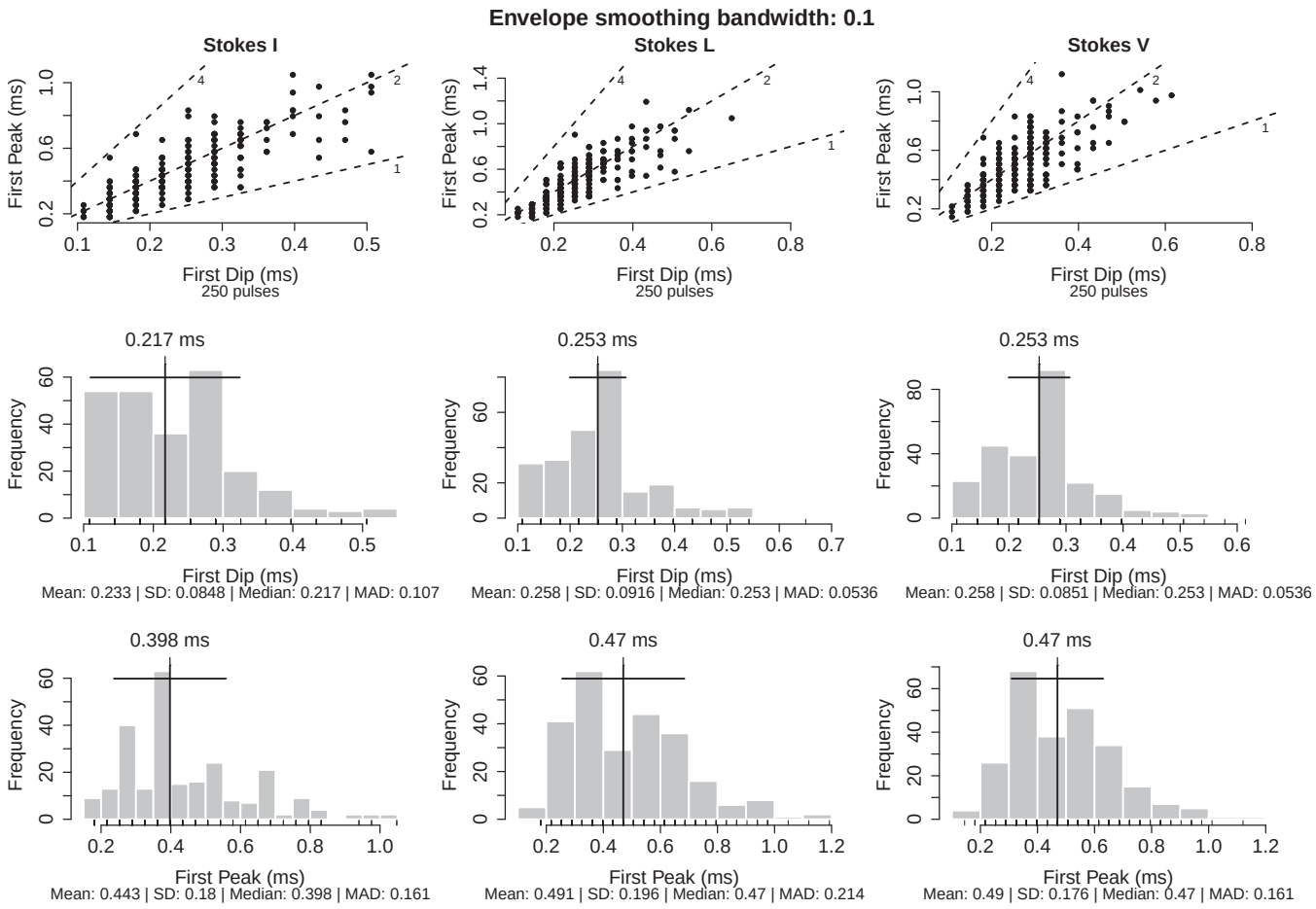
Envelope smoothing bandwidth: 0.1
Stokes I
Stokes L
Stokes V
First Peak (ms)
First Dip (ms)
250 pulses
0.217 ms
0.253 ms
0.253 ms
Frequency
Mean: 0.233 | SD: 0.0848 | Median: 0.217 | MAD: 0.107
Mean: 0.258 | SD: 0.0916 | Median: 0.253 | MAD: 0.0536
Mean: 0.258 | SD: 0.0851 | Median: 0.253 | MAD: 0.0536
0.398 ms
0.47 ms
0.47 ms
First Peak (ms)
Mean: 0.443 | SD: 0.18 | Median: 0.398 | MAD: 0.161
Mean: 0.491 | SD: 0.196 | Median: 0.47 | MAD: 0.214
Mean: 0.49 | SD: 0.176 | Median: 0.47 | MAD: 0.161

Figure 6. The lower three panels are histograms of the estimated time scales of the microstructure signals and similar to fig. 6 of MAR15. The upper plots of these three panels show the relation between the first dip and the first peak in the ACF, the middle shows the distribution of the first dip in the ACF and the bottom panel shows the distribution of the first peak in the ACF which is P_μ. For a detailed description of the technique refer to MAR15.

Rankin (2015, MAR15 hereafter). The top panels of Fig. 5 and 6 show the analysis steps of a single 1.5-GHz pulse as a typical example of microstructure. A quantitative analysis of the pulsar's microstructure properties as carried out by MAR15 was performed on the strong core component, and the periodicities obtained for the smoothing parameter $h = 0.1$ were $P_\mu^I \sim 0.4 \pm 0.2$, $P_\mu^L \sim 0.47 \pm 0.2$, $P_\mu^V \sim 0.47 \pm 0.2$ msec, respectively. MAR15 found a relation for P_μ that increases with increasing pulsar period P for $h = 0.1$ as $P_\mu(msec) = 1.3 \times 10^{-3} P + 0.04$, predicting a value of about 500 μsec for PSR B1933+16, which is in very good agreement with the estimated P_μ. The single pulses at 4.5 GHz were relatively weaker and the microstructure analysis could only be done reliably for Stokes I which yielded $P_\mu^I = 0.35 \pm 0.16$ msec for $h = 0.1$.

One of the reasons that motivated the microstructure study was that PSR B1933+16 is the only truly bright core dominated pulsar in the Arecibo sky, and no published study of microstructure seems to specifically address bright core emission. The comprehensive Arecibo study of broad microstructure in MAR15 treats almost all cone-dominated stars. However, we find a striking similarity between the timescale observed for B1933+16's core component and those for bright conal emission.

Table 1. A/R radio emission heights for pulsar PSR B1933+16, computed as $r = -cP/4\ \phi_c(^\circ)/360$

Component	ν_{obs} (GHz)	ϕ_l (°)	ϕ_t (°)	ϕ_c (°)	r (km)
Core	4.5	–5.4	0.16	–2.78	207
Inner Cone	4.5	–10.0	3.9	–3.05	227
Outer edge	4.5	–14.8	11.4	–3.4	253
Core	1.5	–6.1	0.00	–3.05	227
Inner Cone	1.5	–10.9	4.5	–3.2	238
Outer edge	1.5	–16.8	11.6	–2.6	193

8 CONAL AND CORE EMISSION CHARACTERISTICS

Few opportunities exist to study the properties of the conal emission in core-single $\mathbf{S}_t$ pulsars because the conal outriders appear only at high frequency where the overall emission already tends to be weak relative to meter wavelengths. So it is interesting to carry out some single-pulse polarimetric analyses on the conal portions of B1933+16's 1.5-GHz profile.

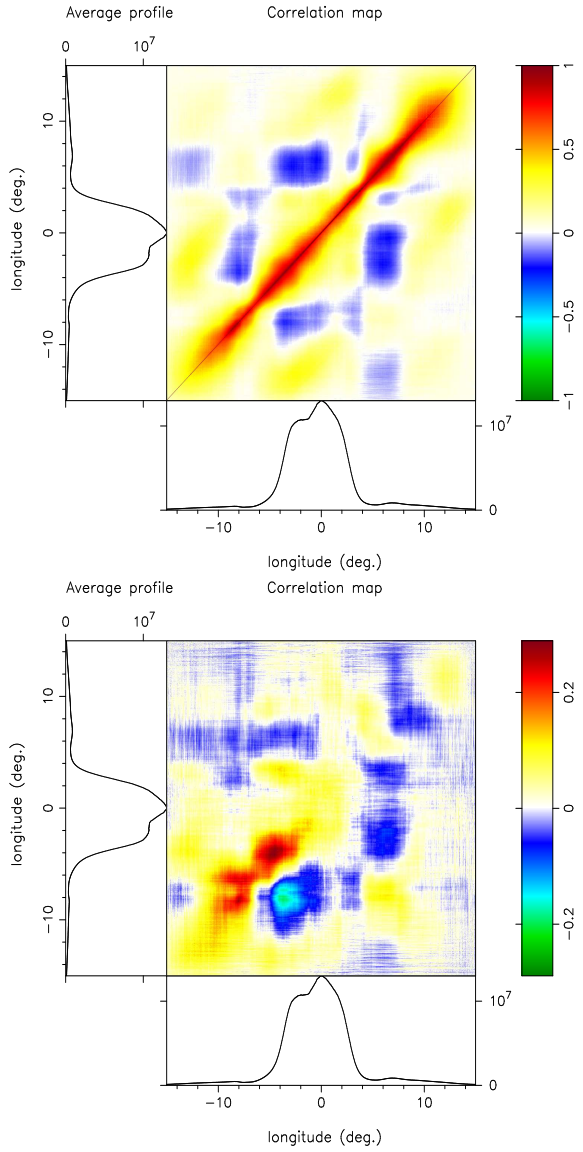

Figure 7. Longitude-longitude correlation displays for zero delay (top) and a one-pulse delay (bottom). The regions on each side of the diagonal are identical in the first plot, and in the second the upper region gives delay +1 and the lower delay –1. Side and lower panels show the average profile for reference. The 3-sigma error in the correlations is about 4%.

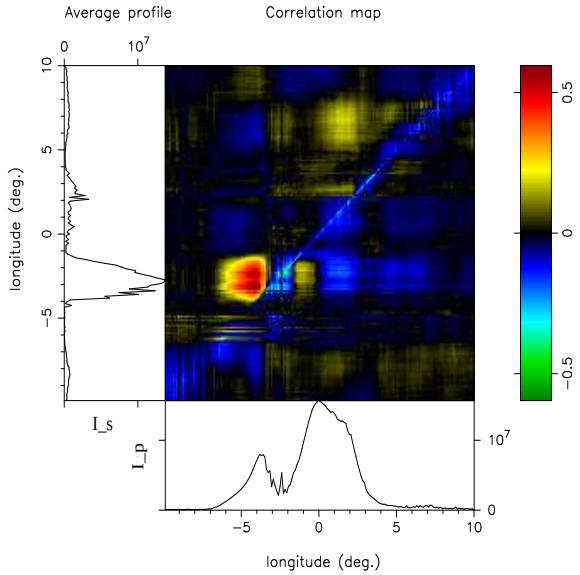

Figure 8. Longitude-longitude cross-correlation display at zero delay between the three-way separated primary and secondary OPM power. Side and lower panels show the average model profiles (as in Figure 4) for reference. The 3-sigma error in the correlations is again about 4%.

In order to study the dynamics of the component structure we computed a longitude-longitude correlation diagram at zero delay, and this is shown in the top panel of Fig. 7. Along the diagonal of complete correlation, several regions are seen that correspond to the leading conal, core and trailing conal parts of the profile. The core feature shows as a rectangle of weak positive correlation (yellow) bounded by weak negative (blue). The conal regions show similar regions of correlation and interestingly the trailing conal region seems to bifurcate into an inner and outer region as discussed above.

The lower display in Fig. 7 computes the correlation at one-pulse delay, and note that the region above the diagonal is no longer a mirror of that below because the upper portion gives the correlations at a delay of +1 pulse and the lower at –1. The region of large positive correlation at about –4° longitude falls on the diagonal and the correlation here is perceptible to delays as long as 5-10 pulses. The area of large negative correlation associates the leading part of the core with the leading conal component, and this changes greatly with increasing delay.

We also carried out fluctuation spectra on the leading and trailing conal regions, but these show no strong periodicities. We see no hint of intensity-dependent effects as in the core. The longitude-longitude correlations do hint at subpulse motion, but not in a very regular manner as in some slower pulsars. It is not very surprising that we see no regular conal modulation, as such "drift" modulation seems almost never to occur in stars rotating as rapidly as B1933+16.

Returning to core properties, Fig. 8 displays the correlation between the 3-way separated primary and secondary modal power. The two different modal profiles that earlier appeared in Fig. 4 are shown in the side and bottom panels for reference. First note the bright positive correlation in the early part of the core feature around –4° that represents the modal fractions of power in this region fluctuating together. Also important are the weaker regions of positive and negative correlation showing how the later primary-mode core radiation is coupled dynamically to the earlier power in the secondary mode.

9 ABERRATION/RETARDATION AND GEOMETRICAL EMISSION HEIGHTS

Pulsar B1933+16 exhibits a core-cone geometry. The prominent conal peaks are seen clearly at 4.5 GHz adjacent to the central core component. At 1.5 GHz the low level conal emission extends far on both the leading and trailing sides of the

profile, however no clear outer conal peaks are discernible. Our analysis of the segregated modes exhibits the largely RVM character of the PPA traverse, and this prompts us to estimate the emission heights (r) for both the core and conal radiation using the A/R method.

In this method the height r can be determined according to the A/R shift $\Delta t{=}4r/c$ [$=\Delta\phi P/360^\circ$], where P is the pulsar period in seconds and $\Delta\phi$ is the longitude difference in degrees between the center of the core or cone emission obtained from the total intensity profiles and the steepest gradient point of the PPA traverse (*i.e.,* Blaskiewicz *et al.* 1991; Mitra & Li 2004; Dyks 2008). $\Delta\phi$ requires determination of the profile center in terms of the longitude difference between a trailing feature ϕ_t and its leading counterpart ϕ_t, such that $\Delta\phi = \phi_c - \phi_0$ where $\phi_c = \phi_l + (\phi_t - \phi_l)/2$ and ϕ_0 is the "fiducial" longitude at the steepest gradient point. Several assumptions and systematic errors are associated with ϕ_l, ϕ_t and ϕ_0 measurements as discussed in Mitra & Li (2004). Also, the A/R method usually assumes an RVM PPA traverse from a single emission height. Aggregate emission from several heights could compromise interpretation of the SG point. Our purpose here, however, is to estimate emission heights which are small compared to the light-cylinder radius.

We apply the A/R method first to B1933+16's conal emission. At 1.5 GHz the peak location of the inner conal emission based on the average profile was not easily discernible. Rather in some low S/N intensity-segregated profiles the peaks of the cone were visible, and we used these locations to identify the center of the cone. The situation is relatively simple at 4.5 GHz where the conal peaks are prominent. We use the profiles in Fig. 1 which are plotted in a manner such that the longitude origin is taken at ϕ_0 and estimate ϕ_l and ϕ_t for the conal peaks of the inner cone. Additionally we also measure ϕ_l and ϕ_t at the extreme outer edges of the profile at an intensity level of five times that of the noise level. These profile measures are given in Table 1, including the estimated emission heights. The errors in the ϕ_l and ϕ_t measurements are much smaller than the systematic errors in this analysis. Typically we find the conal emission heights to be about 200 km above the neutron star surface.

Next we proceed to determine the core emission height using A/R. We estimate ϕ_l and ϕ_t using the half power points on either side of the core feature for both the frequencies. It is interesting to see that the midpoint ϕ_c falls close to the zero-crossing point of the sign changing circular. The resulting emission heights that we obtain are again about 200 km (see Table 1)—very similar to the conal emission heights. This is a remarkable result. For the first time we have successfully been able to apply the A/R tools to estimate the physical emission heights for both the core and conal radio emission regions within the profile.

10 FREQUENCY-INDEPENDENT OPM EMISSION

In general PPA measurements reflect the orientation of the linear polarization electric vector with respect to a reference direction. In our case we measure the PPAs at 1.5 and 4.5 GHz in an absolute sense (Fig. 1), which essentially means that the PPA values at these two frequencies represent the position angle of the linear polarization with respect to celestial North as the emission detaches from the pulsar magnetosphere. As a result, comparison of the PPAs across the profile allows us to directly investigate the frequency evolution of the direction of the linear polarization for a broad frequency range.

For PSR B1933+16 the PPA comparison is not straightforward due to the complex nature of the polarization distributions (see §3). In the central core region between –8° and 0°, the PPA distributions appear to be wildly different at the two frequencies. Particularly the PPAs near –5° longitude are concentrated around –50° at 1.5 GHz and about –30° at 4.5 GHz. The rest of the PPA distribution earlier than about –8° and later than 0° longitude correspond to the conal emission and shows remarkable similarity between the two frequencies. The PPA "patch" at longitude –10° is about PPA –60° and that at longitude +5° about –45°—and these are virtually invariant with frequency. Also the RVM fit that was obtained using at 1.5-GHz PPA traverse (as shown in Fig. 1) fits the PPAs at 4.5 GHz in the conal regions well.

We found an even lower frequency polarization measurement for PSR B1933+16 at 774 MHz by Han *et al.* (2009). Although the paper does not explicitly state that their PPA measurements were calibrated in an absolute sense, the lead author confirms that they were so (Han 2016). Their PPAs below the leading conal component fall at about –65° and those of the trailing at about –50°, so they compare quite closely with our values at 1.4 and 4.5 GHz. Of course, this situation was constructed by measuring the Faraday rotation and derotating the PPAs to infinite frequency in order to achieve the "absolute" calibration. However, it is important here to reverse the question in order to ask what the broad band PPA alignment indicates about the propagation of radiation through the pulsar magnetosphere.

11 ON THE STRUCTURE OF CORE COMPONENTS

The obvious composite structure of B1933+16's core component has long been perplexing. An idea had developed that core components would be Gaussian shaped, however those we have studied closely are not, and perhaps the poor resolution of many older observations had contributed to this incorrect view. In any case we must now attempt to interpret the origins of this structure

The two parts of B1933+16's core component are clearly demarcated by their differing circular and linear polarization in Figs. 1 and 2. The trailing half of the feature has positive circular and substantial linear, whereas the leading half is linearly depolarized and shows negative circular. In earlier work we at some points tried to understand this two part structure in terms of a missing "notch", but we now see strong evidence that the leading and trailing parts of the core have very different polarizations and dynamics.

Paper ET VI interpreted the trailing part of the core as corresponding to the full width of the polar cap. The core width there was measured as twice the peak to trailing half power point or some 4.3°, suggesting a nearly orthogonal value of α (77°). The full core feature width suggested a less

Table 2. Summary of A/R core and conal emission heights as in Table 1 for several pulsars in the literature.

Pulsar	P (s)	$\dot{P}$ (10^{-15} s/s)	**Component**	ν_{obs} (GHz)	ϕ_l (°)	ϕ_t (°)	ϕ_c (°)	r (km)	Ref
B0329+54	0.714	2.05	Core	0.3			–1.5 ± 0.2	223±30	MRG07
			Inner peaks	0.3	–6.2±0.2	5.0±0.2	–0.7±0.2	104±30	
			Outer peaks	0.3	–13.8±0.2	10.0±0.2	–1.9±0.2	282±30	
B0355+54	0.156	4.4	Core	0.3	–15.0 ± 0.5	–8.0 ±0.5	–11.5±0.5	373±15	MR11
			Outer peaks		–39.7 ± 0.5	–9.3 ± 0.4	–15.2±0.6	494±19	
B0450+55	0.340	2.37	Core	0.3	–14.5 ± 0.5	–7.5 ±0.5	–11.0±0.5	779±35	MR11
			Outer peaks	0.3	18.5 ± 0.2	10.8 ±0.2	–3.9 ±0.2	274±12	
B1237+25	1.382	9.06	Core	0.3			–0.4±0.1	117±30	ERM14
			Inner peaks		–4.0±0.2	3.3±0.2	–0.35±0.2	101±50	
			Outer peaks		–6.4±0.2	5.1±0.2	–0.6±0.2	172±50	

References: MRG07, Mitra, Rankin & Gupta (2007); MR11, Mitra & Rankin (2011); ERM13, Smith, Rankin & Mitra (2013).

Table 3. Summary of plasma properties for core and conal emission. The frequency ν_B is the cyclotron frequency estimated for $\gamma_s = 200$, frequency ν_p estimated for $\gamma_s = 200$ and two values of $\kappa = 100, 10^4$, the cyclotron frequency estimated for two values of $\Gamma_s = 300, 600$. The radius of the light cylinder is given by $R_{lc} = cP/2\pi$ and the height of the radio emission r in terms of light cylinder distance is given by $R = r/R_{lc}$. The quantities $\Psi = PA_v - PA_\circ$, measured for the primary Ψ_{PPM} and secondary Ψ_{SPM} polarization modes, are obtained from Rankin (2015).

Pulsar	P (s)	$\dot{P}$ (10^{-15} s/s)	**Component**	ν_{obs} (GHz)	ν_B (GHz)	ν_p (GHz)	ν_{cr} (GHz)	R	R_{lc} (km)	Ψ_{PPM} (°)	Ψ_{SPM} (°)
B1933+16	0.358	6.0	Core	4.5	4676	20−200	0.5−4.3	0.01	17093	+112(5)	+22(5)
			Inner Cone	4.5	3545	17−174	0.4−4.2	0.01			
			Outer edge	4.5	2561	15−148	0.5−3.9	0.01			
			Core	1.5	3545	17−174	0.4−4.2	0.01			
			Inner Cone	1.5	3076	16−162	0.5−4.1	0.01			
			Outer edge	1.5	5769	22−222	0.5−4.5	0.01			
B0355+54	0.156	4.4	Core	0.3	451	9.4−94.4	0.6−4.9	0.05	7448	+89(5)	–1(5)
			Outer peaks		195	6.1−62	0.5−4.2	0.07			
B0450+55	0.340	2.37	Core	0.3	54	2.2−22	0.3−2.3	0.05	16233	+86(16)	–4(16)
			Outer peaks	0.3	1234	10−105	0.5−3.9	0.02			
B0329+54	0.714	2.05	Core	0.3	3087	11−115	0.4−3	0.006	34090	+99(4)	+9(4)
			Inner peaks	0.3	30438	36−362	0.5−4.3	0.003			
			Outer peaks	0.3	1526	8−81	0.3−2.6	0.008			
B1237+25	1.382	9.06	Core	0.3	19910	21−210	0.4−3.0	0.002	65890	+143(4)	+53(4)
			Inner peaks	0.3	30612	26−261	0.4−3.1	0.002			
			Outer peaks	0.3	6198	11−117	0.3−2.5	0.002			

orthogonal geometry which appeared incompatible quantitatively with the steep R_{PA}. The issue remains here: we fitted Gaussians to the pulsar's 1.5-GHz profile, finding that the central core region was well fitted by two Gaussians, the trailing one with a halfwidth of about 4.5-5°, and a leading one some 3° earlier of about 2° halfwidth and half the amplitude. This analysis is then compatible with the earlier assumption that the trailing region is associated with the full polar cap emission and that the leading feature is "something extra".

This line of interpretation is also compatible with the more complete, probably X-mode linear polarization of the trailing region—and seen in many other core features (ET XI)—and the complex, depolarized largely O-mode emission in the earlier part. The polarization mixing around –5° longitude results in the strongly diverted average PPA traverse and coincides with the peak of the leading fitted "extra" Gaussian above. Both polarization modes are clearly present in this region and mix both to produce the linear depolarization and the splay of different polarization states seen in individual samples. Further, we have seen that higher resolution exhibits the diversion of the average PPA in this region ever more strongly, so the "extra" emission in this narrow region is probably O mode such that its "patch" of PPAs in Fig. 1 (upper) would fall on the modal RVM track if our resolution was even higher.

The distinction between the trailing core region and the "extra" leading emission is also seen in the contrasting forms of the mode-segregated profiles. We can also see that something peculiar is happening dynamically at –5° longitude in the persistent correlation at 1-pulse delay (Fig. 7 lower), and this effect is further clarified in Fig. 8 where strong positive correlation is indicated between the power of the two modes in this region. However, it is important to note that the peak falls well off the diagonal of the diagram, indicating correlation between the modal power at different longitudes.

Our earlier pulse-sequence polarimetric studies of core emission in pulsars B0329+54 (Mitra *et al.* 2007) and B1237+25 (Smith *et al.* 2013) also exhibited core features of two parts, marked by distinct leading and trailing regions of modal emission and hands of circular polarization. Our analyses of these two pulsars went in somewhat different directions because their cores were modulated by intensity-dependent A/R, whereas B1933+16's emission is much steadier. A further difference was that the "extra" leading emission had smaller relative intensity, so that the core width could be directly interpreted geometrically.

12 SUMMARY

Using high resolution polarimetric Arecibo observations of pulsar B1933+16 at 1.5 and 4.6 GHz, we have conducted a comprehensive analysis of this brightest core dominated pulsar in the Arecibo sky. Here we summarize the main results W of our analysis:

- With the exception of one region near –5° longitude, the 1.5-GHz PPA traverse can be well fitted by an RVM curve. This shows that most of the core power is in the primary mode and most of the conal in the secondary.
- The 4.6-GHz core polarization is much more difficult to interpret, whereas the conal PPAs are nearly identical to their counterparts at 1.5 GHz. Imposing the 1.5-GHz RVM fit on the 4.6-GHz PPA provides useful insight on how the latter should be interpreted.
- High resolution analysis reveals the apparently non-RVM region of emission at about –5° longitude with unprecedented clarity.
- The 1.5-GHz RVM fit gives α and β values of 125°and –1.2°, respectively, with large errors due to the nearly complete correlation between them. The resulting PPA at the inflection point is –58°±5°, where we have taken the longitude origin in our various plots. See Fig. 1. Efforts were made to interpret the several different core and conal modal "patches" in different ways, and we believe the above fit properly represents the pulsar's actual emission geometry.
- Such a "fiducial" PPA of –58° together with the measured PA_v direction of +176(0)° indicates polarization orientation +54°±5°. Despite this measured cant from 90°, we believe that it probably still identifies the extraordinary (X) propagation mode.
- An intensity-fractionation analysis showed only weak differences in the several populations of pulses in B1933+16, in large part because the pulsar emission tends to be very steady from pulse to pulse. See Fig. 2.
- However, B1933+16's core structure is similar to that seen before in B0329+54 and B1237+25—that is, it shows a double modal structure with both opposite senses of circular polarization and orthogonal linear polarization. In these other pulsars, the two parts are strongly correlated dynamically, but the connection is less apparent in B1933+16 due to its steady intensity from pulse to pulse. Fig. 8, however, shows the highly correlated mixed-mode power early and its bridge to the later X-mode emission.
- The 1.5-GHz modal emission was segregated using both the two- and three-way techniques as seen in Figs. 3 and 4. These show that the later parts of the core are dominated by X-mode emission, whereas the earlier parts represent the O mode.
- Analysis of broad microstructures in the emission of B1933+16's core component shows that their timescales are nearly identical with the similar largely conal emissions studied earlier—-in this case some 500 μsec. See Fig. 5 & 6.
- Longitude-longitude correlations and fluctuation-spectral analyses of B1933+16's 1.5-GHz emission show distinct conal and core regions. The former again show a mix of inner and outer conal radiation. Fluctuation spectra provide no signs of periodicity.
- Aberration/retardation analyses provide physical emission height measurements for B1933+16's conal emission and unusually here for its core radiation as well. These computations in Table 1 suggest that both the conal and core radiation stems from an average height of around 200 km above the neutron-star surface.
- Conal linear polarization in B1933+16 exhibits very similar absolute PPAs between 0.77 and 4.6 GHz after derotating them according to the small interstellar Faraday rotation exhibited by the pulsar.

13 THEORETICAL INTERPRETATION AND DISCUSSION

The enormous brightness temperatures of pulsar radio emission demand a coherent plasma radiation mechanism. Relating physical theories of coherent radio emission to the observations requires above all else one crucial datum: the location of the regions within the magnetosphere where the core and conal radio emission are emitted. The A/R method for determining radio emission heights is physically grounded and little model dependent, but it has been successfully applied more to the conal emission, where the RVM can more usually be fitted to conal PPA traverses and the SG points accurately determined. Cores have too often presented complex traverses for which it could be doubted whether an RVM fit was appropriate or even possible. Some earlier efforts were made to measure A/R heights for cores (Mitra & Li 2004), but the results have remained inconclusive and in some cases seemed to show the wrong sense.

In an effort to resolve important questions about cores—and their emission heights in particular—we have embarked on a systematic study of pulsars with bright core components as well as prominent conal emission. This paper is the third in a series that began with pulsar B0329+54 (Mitra, Rankin & Gupta 2007) and then studied B1237+25 (Smith, Rankin & Mitra 2013). Each of the pulsars exhibits distinct conal and central core emission components along with a complex PPA traverse. By using high quality single pulse polarimetry and PPA mode segregation techniques, we

were able to identify the underlying RVM as we did earlier for B0329+54.

This in turn permitted us to estimate the core and conal A/R shifts that are here summarized in Table 2 (refer to notes in the Table for details about individual measurements). Amongst these three pulsars PSR B1933+16 is the fastest and has the best determined A/R shift. We searched the literature and found that for two more pulsars, PSR B0355+54 and PSR B0450+55, the A/R-based core and conal shifts could be determined with confidence—*i.e.,* we could identify their components clearly as core or conal and then fit the RVM to their PPA traverses. As seen in Table 2 the conal and core centers $\Delta\phi_c$ lead the SG point in each case, which in turn suggests that the core and conal emission arises from a finite heights above the polar cap. However, unlike for B1933+16, the core and conal centers do not coincide, and hence the A/R shift method, using the simple relation $r = c\Delta\phi P/4 \times 360^\circ$, cannot be used to estimate these emission heights accurately. There can be a few reasons for this, for example: the methods employed to measure the emission centers are not sufficiently accurate (see Mitra & Li 2004); the emission patterns are not centered about the dipole axis: or finally the core and conal emission arises from different heights. Our aim here, however, is not to find exact emission heights, but to illustrate that the radiation arises from deep within the magnetosphere at altitudes of a few hundred kilometers. In this spirit we simply estimate the core and conal emission heights r in Table 2 assuming their centers are shifted by A/R. However, the excellent RVM fits to the PPA traverses in all these cases also implies that the height differences between the core and conal emission must be relatively small, as large differences can cause distortions and kinks in the PPA traverse (see Mitra & Seiradakis 2004).

These measurements, taken together, provide definitive evidence, we believe, that the core and conal (hence all) radio emission arises in regions at heights of typically no more than a few hundred kilometers above the neutron-star surface. .

Although the PPA traverses of these pulsars are complex and heretofore inscrutable in RVM terms, our techniques of high resolution polarimetry, intensity fractionation and modal segregation have been able to reliably identify their underlying RVM traverses. B1933+16 was the most complex in these terms we have studied, and we began our work presuming that its traverse must entail a coherent combination of polarized power to so distort its observed PPA traverse. However, as we have seen, this is not the case: the non-RVM distortions in each of these pulsars are primarily polarization-modal in origin. The two orthogonal polarization (PPM and SPM) modes undergo incoherent mixing of varying intensities and degrees of orthogonality across the pulse profile—with the mixing occurring on such short timescales that our high resolution observations can partially resolve them. These effects are particularly acute in the core emission, and there also complicated by intensity-dependent A/R.

Our ability to trace the PPM and the SPM across the profile and to identify them with the absolute $PA_\circ$ together with the PA_v direction further permits us to associate the OPMs with the X and O propagation modes in the pulsar magnetosphere. This is then summarized in Table 3. For pulsars B0329+54, B0355+54 and PSR B0450+55 the association of the PPM with the X and the SPM with the O mode is very good. This is in general agreement with the measured Ψ distribution for core dominated pulsars (Rankin 2015) where the PPM emission for core components is associated with the X mode. For PSR B1933+16 the association is less precise and B1237+25's canted orientation may stem from its position near the North Galactic pole.[1] In any case, the observations now strongly suggest that the emission emerging from the pulsar magnetosphere is comprised of the X and O modes.

The observational evidence locating the pulsar radio-emission region and associating the radiation with the X and O plasma modes have strengthened our ability to identify the curvature-radiation mechanism as responsible for exciting coherent radio emission in pulsars (*e.g.,* Melikidze, Gil & Pataraya 2000, hereafter MGP00; Gil, Luybarski & Meikidze 2004, hereafter GLM04; Mitra, Gil & Melikidze 2009; Melikidze, Mitra & Gil 2014, hereafter MMG14). In most pulsar emission models the the rotating neutron star is a unipolar inductor due to the enormous magnetic fields, and a strong electric field is generated around the star. In such strong electric and magnetic fields charged particles can be pulled out from the neutron star and/or be created by the process of magnetic pair creation. Finally the region around the neutron star becomes a charge-separated magnetosphere which is force free. The physics of how particles populate and flow in the pulsar magnetosphere is a matter of intense research; however, the consensus is now that, in the presence of sufficient plasma, a relativistic plasma flow can be generated along the global open dipolar magnetic field [see Spitkovsky (2011) for a review]. In order to achieve a force-free condition and to maintain corotation the magnetosphere needs a minimum charge density (Goldreich & Julian 1968) of $n_{GJ} = \Omega \cdot B/2\pi c$ (rotational frequency $\Omega = 2\pi/P$, where P is the pulsar period, B is the magnetic field and c is velocity of light). A key aspect of the magnetosphere is that enormous electric fields will be generated in regions depleted below the n_{GJ} value, where the remaining charges can be accelerated to high energies and more charges produced in that region.

In order to explain the origin of pulsar radio emission arising relatively close to the star, a charge-depleted acceleration region just above the polar cap is found to be necessary. Such a prototype region was envisaged as an inner vacuum gap (IVG) by Ruderman & Sutherland (1975, RS75). The gap has strong electric and magnetic fields and is initially charge starved. Apparently, the IVG can eventually discharge as electron-positron pairs in the form of "sparks" at specific locations, and corresponding non-stationary spark-associated relativistic primary particles with Lorentz factors of γ_p can be generated. This dis-

[1] It remains surprising that $PA_v - PA_0$ for many pulsars falls close to either 0 or 90°. Excellent polarimetry and careful analysis has determined PA_0 values for these pulsars with certainty, and the proper-motion directions measured by both VLBI and timing are in good agreement with each other. To the extent that pulsar velocities are due to natal supernova "kicks", the one alignment can be understood, but binary disruption would tend to produce the other. So we have much to learn both about why the alignments tend to be close to 0 or 90° as well as why some show significant misalignments.

charge process continues until the force-free charge density n_{GJ} is reached. The electron-positron pairs are separated due to the electric field in the IVG, and one kind of charge streams outward towards the upper magnetosphere further radiating in the strong magnetic fields and the resulting photons thereby producing secondary electron-positron plasma with Lorentz factor γ_s. Thus the charge density in the outflowing secondary plasma n_s gets multiplied by a factor $\kappa \sim n_s/n_{GJ}$ (Sturrock 1971). The backflowing plasma then heats the polar cap surface and can generate thermal x-ray emission. For the above process to work, the RS75 model assumed a magnetic curvature radius of 10^6 cm in the vacuum gap, which in fact implies strongly non-dipolar fields (see *e.g.,* Gil, Melikidze & Mitra 2004). As a consequence the range for $\gamma_p \sim 10^6$, $\nu_s \sim$ few hundreds, and $\kappa \sim 100 - 10^4$. The RS75 model had some shortcomings, however, as it could not explain the slower-than-expected subpulse-drifting effect (Deshpande & Rankin 2001), and it also predicted higher temperatures for the hot polar caps than were observed. A refinement of the model by GLM04 suggested that a partially screened IVG can be realized that can explain these effects. In any case, the core and conal radio emission are generated through the growth of plasma instabilities in the spark-associated relativistically flowing secondary plasma.

Knowledge of the location of the pulsar emission and using the above model, it is possible to compute the various frequency scales involved in the pulsar emission problem. Following eqs. (10), (11) and (12) in MMG14, the cyclotron frequency ν_B, and plasma frequency ν_p at a fractional light cylinder distance R for a pulsar with period P and $\dot{P} = \dot{P}_{15} \times 10^{-15}$ can be expressed as $\nu_B = 5.2 \times 10^{-2}(1/\gamma_s) \times (\dot{P}_{15}/P^5)^{0.5} R^{-3}$ GHz and $\nu_p = 2 \times 10^{-5}\kappa^{0.5}\sqrt{\gamma_s}(\dot{P}/P^7)^{0.25}R^{-1.5}$ GHz. In Table 3 we provide the values of ν_B and ν_p for a reasonable value of $\gamma_s = 200$ and two values of $\kappa = 100, 10^4$, respectively. For all cases we find $\nu_p < \nu_B$, and further the the observed radio emission $\nu_{obs} < \nu_p$, or in other words the observed frequency of radio emission is lower than the plasma frequency of the emitting plasma.

A model of pulsar radio emission for $\nu_{obs} < \nu_p < \nu_B$ has been developed by MGP00. It is important to notice that the only known instability that can operate at low radio emission heights (typically below 10% of the light cylinder) is the two-stream instability. The non-stationary sparking IVG discharge leads to generation of secondary plasma clouds with slight spreads in their particle velocities. The faster and slower velocities of two successive clouds overlap at the heights of radio emission to trigger strong Langmuir turbulence in the secondary plasma, which can become modulationally unstable. MGP00 demonstrated that nonlinear growth of the modulational instability can lead to formation of charged solitons which are capable of emitting curvature radiation in curved magnetic fields. The soliton size must be larger than the linear Langmuir wave, and to maintain coherence the emission should have wavelengths larger than the soliton size, or in other words $\nu_{obs} < \nu_p$ as observed. The theory suggests that the maximum frequency of the soliton coherent curvature radiaiton given by eq. (12) in MMG14 is $\nu_{cr} = 0.8 \times 10^9(\Gamma^3/P)R^{-0.5}$ GHz, where Γ is the Lorentz factor of the emitting soliton. The value of Γ is slightly different from γ_s, and assuming a two reasonable values of $\Gamma = 300, 600$ we estimate values of ν_{cr} as given in Table 1. Clearly the values lie in the observed frequency range—*i.e.,* $\nu_{cr} \sim \nu_{obs}$.

Finally we turn our attention to the prediction of the coherent curvature radiation theory for the X and O modes and their propagation in the magnetosphere. We have emphasized in §10 that in PSR B1933+16 the linear polarization direction remains unchanged for conal emission between 0.77 and 4.5 GHz. In turn, if we invoke the RVM solution, we can conclude that with respect to the magnetic field line planes there is no rotation or adiabatic walking of the linearly polarized conal modal emission in the pulsar magnetosphere. We note that several current studies suggest the invariance of the PPAs with frequency. One class of investigation involves establishing the rotation measure variation as a function of pulse phase (Ramachandran *et al.* 2004; Noutsos *et al.* 2009), and these studies indicate that the rotation measure across a pulsar's profile is largely due to the interstellar medium. Another study by Karastergiou & Johnston (2006) compared absolute PPAs between 1.4 and 3.1 GHz and found very little change with frequency.

If the PPA modes are interpreted as the X and O modes, then the absence of adiabatic walking, at least for the X mode, can be understood in the framework of the propagation effects predicted by the coherent curvature radiation theory as shown in a recent work by MMG14. This theory demonstrated that for radio emission to be excited and detach from the magnetosphere below 10% of the light cylinder (which is also the case for PSR B1933+16 as shown above), the refractive index of the emitting plasma for the X-mode propagation is unity, and hence the X mode can emerge from the plasma preserving its emitted polarization direction. However the theory has no prediction for the O mode nor for the existence of circular polarization. These appear to be two fundamental problems that need to be resolved in pulsar emission theories as emphasized in the latter paper.

14 CONCLUSION

In this paper we have established that the core and conal emission lie at heights of no more than several hundred kilometers, core and conal emission display similar short timescale microstructures, and their emission can also be associated with the X and O modes. These similarities strongly suggest, as expected, that the core and conal emission processes have the same physical origin. However, we have yet to understand the causes of their individual geometric, polarization and modulation properties. We argue that, overall, the pulsar radio emission mechanism is excited by coherent curvature radiation.

ACKNOWLEDGMENTS

We thank our referee Jarsalow Dyks for providing constructive comments which helped in improving the paper. Much of the work was made possible by support from the NASA Space Grants and from US National Science Foundation grant 09-68296. One of us (JMR) also thanks the Anton Pannekoek Astronomical Institute of the University of Amsterdam for their support. Arecibo Observatory is operated

by SRI International under a cooperative agreement with the US National Science Foundation, and in alliance with SRI, the Ana G. Méndez-Universidad Metropolitana, and the Universities Space Research Association. We thank Prof. Jinlin Han for sharing their 774-MHz polarimetry of PSR B1933+16. This work made use of the NASA ADS astronomical data system.

REFERENCES

Blaskiewcz, M., Cordes, J.M., & Wassermann, I. 1991 Ap.J., 370 643 (BCW)
Deshpande, A.A., Rankin, J.M., 2001, *MNRAS*, 322, 438
Dyks, J., 2008, MNRAS, 391, 859
Everett, J. E., & Weisberg, J. M. 2001, *Ap.J.* , 553, 341
Gil, J., Lyubarski, Y., & Melikidze, G. I. 2004, *Ap.J.* , 600, 872 (GLM04)
Goldreich, P. & Julian, W. H., 1969, *Ap.J.* , 157, 869
Gould, D. M., & Lyne, A. G., 1998, *MNRAS*, 301, 235
Han, J. L. 2016, private communication.
Han, J. L., Demorest, P. B., van Stratten, W., & Lyne, A. G. 2009, *Ap.J.* ,181, 557
Hankins T.H., Rankin J.M., 2010, *A.J.* , 139, 168
Hobbs, G., Lyne, A. G., Kramer, M. 2005, Martin, C. E., & Jordan, C. 2004, *MNRAS*, 353, 1311
Izvekova V. A., Malofeev V. M., & Shitov Yu.P. 1989, Astron. Zh. 66, 345-354
Johnston, S., Hobbs, G., Vigeland, S., Kramer, M., Weisberg, J. M., & Lyne, A. G. 2005, *MNRAS*, 364, 1397
Karastergiou, A., & Johnston, S. 2006, *MNRAS*, 365, 353
Krishnamohan, S., & Downs, G. S. 1983, *Ap.J.* , 265, 372.
Melikidze, G. I., Gil, J., & Pataraya, A. D. 2000, *Ap.J.* , 544, 1081. (MGP00)
Melikidze, G. I., Mitra, D., & Gil, J. 2014, *Ap.J.* , 794, 105. (MMG14)
Mitra, D., Gil, J., & Melikidze, G. I., 2009, *Ap.J.* , 794, 105.
Mitra, D. & Li, X. H., 2004, A&A, 421, 215
Mitra, D., Arjunwadkar, M., & Rankin, J. M. 2015, *Ap.J.* , 806, 236 (MAR15)
Mitra, D., & Rankin, J. M. 2011, *Ap.J.* , 727, 92 (ET IX)
Mitra, D., Rankin, J. M., & Gupta, Y. 2007, *MNRAS*, 379, 932
Mitra, D. & Seiradakis, J. H., 2004, in Laskarides P. G., ed., Proc. 6th Hellenic Astronomical Conference. Univ. Athens, Athens, p. 205
Noutsos, A., Karastergiou, A., Kramer, M., Johnston, S., & Stappers, B. W. 2009, *MNRAS*, 396, 1559
Noutsos, A., Kramer, M., Carr, P., & Johnston, S. 2012, *MNRAS*, 423, 2736
Radhakrishnan, V., & Cooke, D. J. 1969, Ap. Lett, 3, 225
Ramachandran, R., Backer, D. C., Rankin, J. M., Weisberg, J. M., & Devine, K. E .2004, *Ap.J.* , 606, 1167
Rankin, J. M. 1983a, *Ap.J.* , 274, 359 (ET I)
Rankin, J. M. 1983b, *Ap.J.* , 274, 359 (ET II)
Rankin, J. M. 1993a, *Ap.J.* , 405, 285 (ET VIa)
Rankin, J. M. 1993b, *Ap.J. Suppl.* , 85, 145 (ET VIb)
Rankin, J. M. 2015, *Ap.J.* , 804, 112
Rankin, J. M., Stinebring, D. R., & Weisberg, J. M. 1989, *Ap.J.* , 346, 869
Ruderman, M. A., & Sutherland, P. G. 1975, *Ap.J.* , 196, 51
Sieber, W., Reinecke, R., & Wielebinski, R. 1975, *A&A* , 38, 169
Smith, E. M., Rankin, J. M., & Mitra, D. 2013, *MNRAS*, 435, 1984.
Spitkovsky, A, 2011, HEEP, editor Torres, D. F & Rea, N., 139
Sturrock, P. A., 1971, *Ap.J.* , 164, 129
Weisberg, J. M., Cordes, J. M., Lundgren, S. C., Dawson, B. R., Despotes, J. T., Morgan, J. J., Weitz, K. A., Zink, E. C., & Backer, D. C. 1999, *Ap.J. Suppl.* , 121, 171